Cement and Concrete Research 41 (2011) 1–8

Contents lists available at ScienceDirect

Cement and Concrete Research

journal homepage: http://ees.elsevier.com/CEMCON/default.asp

Effect of binder content on the performance of alkali-activated slag concretes

Susan A. Bernal [a,*], Ruby Mejía de Gutiérrez [a], Alba L. Pedraza [a], John L. Provis [b,*], Erich D. Rodriguez [a,1], Silvio Delvasto [a]

[a] Materials Engineering Department, Composite Materials Group, CENM, Universidad del Valle, Cali, Colombia
[b] Department of Chemical and Biomolecular Engineering, University of Melbourne, Victoria 3010, Australia

ARTICLE INFO

Article history:
Received 26 May 2010
Accepted 31 August 2010

Keywords:
Alkali-activated cement (D)
Mixture proportioning (A)
Mechanical properties (C)
Capillary sorptivity
Carbonation (C)

ABSTRACT

This paper assesses the mechanical and durability performance of concretes produced using alkali silicate-activated ground granulated blast furnace slag as sole binder. Alkali-activated concretes are formulated with 300, 400 and 500 kg slag per m^3 of fresh concrete, and their performance is compared with reference concretes produced using Portland cement (OPCC). Regardless of the binder content, the alkali-activated slag concretes (AASC) develop higher compressive strength than the comparable reference concretes. A higher binder content leads to increased strength in both AASC and OPCC at 28 days. However, at 90 days, the performance penalty for low binder content is more significant in the OPCC than AASC samples. Permeability, water sorption and carbonation resistance properties are also improved at higher binder contents. By controlling mix design parameters, it is possible to produce AASC with mechanical strength and durability comparable to conventional Portland cement concretes.

1. Introduction

Alkali-activated concretes are a new generation of alternative building materials, whose main difference from traditional Portland cement concretes is the use of a relatively alkali-rich, clinker-free binder matrix such as alkali-activated slag or geopolymer. Compared with conventional concretes, the production of alkali-activated concretes is associated with low energy consumption and low CO_2 emission, along with the potential to reach high mechanical strength at early ages of curing, high stability in aggressive environments and resistance to elevated temperatures, among others [1–5]. These properties have made concretes based on alkali-activated binders a very interesting alternative from both scientific and commercial points of view [3,6,7]. Commercialisation of alkali activation technology is moving forward on most continents, and the development of alkali-activated binders is a highly active area of academic and industrial research.

However, there are few reports in the academic literature regarding the engineering and durability properties of alkali-activated concretes, as opposed to mortar or paste samples [8–16]. This suggests that there is not yet a full understanding of the effect of the mix design parameters of alkali-activated concrete on the mechanical strength and long-term durability of the resulting materials. It is important to note that the variability in the composition and reactivity of the different potential precursors that can be used to produce these materials, has meant that it has not yet been possible to establish an international standard (prescriptive) design procedure for alkali-activated concrete mixes, in order to reach a specific performance level over a designated service life. The available reports related to alkali-activated concretes based on metallurgical slags have shown that in addition to the effect of the binder chemistry and the activation process itself, concrete mix design parameters such as the amount of binder and the water/binder ratio may strongly affect the mechanical strength and the durability of the final products [3,16,17].

Understanding the durability of any building material when exposed to aggressive environments is critical in predicting how the material will behave in service. Carbon dioxide (CO_2) is one agent that may drastically affect the long-term durability of concrete structures. This phenomenon is usually referred to as carbonation, leads to a loss of alkalinity and the degradation of embedded steel reinforcing, and is one of the main causes of damage to civil infrastructure [18–23]. In the case of alkali-activated concretes, being materials which are only now beginning to be brought into service in most parts of the world, there is little existing knowledge about the long-term in-service stability of these materials. However, experience in Poland, Ukraine and Russia has generally shown good durability in service [24–27].

Studies carried out using pastes and mortars of alkali-activated slag, and slag/metakaolin blends, have revealed that these materials present a potentially higher susceptibility to carbonation compared with conventional cements, as a consequence of the differences in the mechanism of degradation and their microstructure [26,28–31]. It has been identified

* Corresponding authors. S.A. Bernal is to be contacted at Instrument Centre for Solid-State NMR Spectroscopy and Interdisciplinary Nanoscience Center, Department of Chemistry, Aarhus University, DK-8000 Aarhus C, Denmark. Tel.: +61 3 8344 8755; fax: +61 3 8344 4153. Provis, Tel.: +61 3 8344 8755; fax: +61 3 8344 4153.
E-mail addresses: susana.bernal@gmail.com (S.A. Bernal), jprovis@unimelb.edu.au (J.L. Provis).
[1] Current address: Instituto de Ciencia y Tecnología del Hormigón, Universidad Politécnica de Valencia, 46022 Valencia, Spain.

0008-8846/$ – see front matter © 2010 Elsevier Ltd. All rights reserved.
doi:10.1016/j.cemconres.2010.08.017

Table 1
Chemical composition of GBFS and OPC used. LOI is loss on ignition at 1000 °C.

Type of binder	Component (mass % as oxide)							
	SiO_2	Al_2O_3	CaO	Fe_2O_3	MgO	TiO_2	Na_2O	LOI
GBFS	33.70	12.80	45.40	0.96	1.00	0.50	0.14	2.72
OPC	20.35	6.06	57.06	4.58	3.10	–	–	5.80

that this behavior is also dependent on the nature of the alkali activator used [30,32], being more significant when silicate activators are used to produce the binders. However, silicate-activated slag binders are very attractive compared to those produced with other activators (hydroxides, carbonates, sulfates) because of the potential to achieve high mechanical strengths [15].

The rate of carbonation of a concrete is mainly determined by the physical properties of the solid binder, in particular porosity and permeability, and also by the specific details of the chemistry of the binder phase including its susceptibility to decalcification [23,33–35]. For conventional cement-based materials, these properties can be improved by modifying the concrete mixes to enhance particle packing and the properties of the interfacial transition zone; however, the study of similar processes in alkali silicate-activated slag concretes has not previously been reported. Thus, there is certainly the need to develop a better understanding of the effects on mechanical strength and sorptivity properties of mix design parameters of alkali silicate-activated slag concretes. This will enable the design of concretes with improved durability. The key mix design parameter investigated in this study is the binder content of the concrete, which is a parameter whose influence on Portland cement concretes is very well understood but which has not been studied systematically for the case of alkali-activated slag concretes.

2. Experimental program

2.1. Materials

The starting material used to produce the binder is a Colombian granulated blast furnace slag (GBFS) from the factory *Acerías Paz del Río*. The basicity coefficient ($K_b = CaO + MgO/SiO_2 + Al_2O_3$) and the quality coefficient ($CaO + MgO + Al_2O_3/SiO_2 + TiO_2$) based on the chemical composition (Table 1) were 1.01 and 1.92, respectively. Its specific gravity and Blaine fineness were 2900 kg/m^3 and 399 m^2/kg, respectively. The particle size range determined by laser granulometry was 0.1–74 μm, with a D_{50} of 5 μm. A commercial ordinary Portland cement (OPC) type I with a Blaine fineness of 363 m^2/kg and a specific gravity of 3030 kg/m^3 was used as reference binder. This cement was provided with a 10% limestone admixture and its chemical composition is shown in Table 1.

The alkaline activation of the GBFS was carried out using a commercial sodium silicate solution ($Na_2O.rSiO_2\,nH_2O$) composed of 32.4% SiO_2, 13.5% Na_2O and 54.1% H_2O by mass. The silica modulus of the solution (M_s = molar SiO_2/Na_2O ratio) was 2.4.

Crushed gravel and river sand were used as coarse and fine aggregates in the manufacture of concrete. The coarse aggregate was of 19 mm maximum size, specific gravity of 2790 kg/m^3 and absorption of 1.23%. The specific gravity, absorption, and fineness modulus of the sand were 2450 kg/m^3, 3.75% and 2.57, respectively.

2.2. Experimental program

2.2.1. Concrete mixes

Alkali-activated slag concretes (AASC) were produced with slag contents of 300, 400 and 500 kg per cubic meter of fresh mixture, corresponding to total binder (slag + anhydrous activator) contents of 351, 468 and 585 kg/m^3 respectively (Table 2). The mixes were formulated to achieve initial slump flow consistency of around 70 mm and a total water/slag ratio of 0.42. The alkaline activator was incorporated at a concentration of activation of 5% Na_2O (i.e., 5 g Na_2O per 100 g slag). The control specimens of OPC concretes were designed following the standard procedure ACI 211.1–91 (*Standard Practice for Selecting Proportions for Normal, Heavyweight and Mass Concrete*), using the same amounts of cement and the same water/binder ratio specified for the alkali-activated concretes. It is important to note that OPC concrete specimens were cured under water at ambient laboratory conditions (25 °C), while alkali-activated concretes were kept in a humidity-controlled chamber (relative humidity of 90% RH) at 25 ± 5 °C in order to prevent leaching of the alkaline activator.

2.3. Tests conducted on concretes

Concrete samples were tested to determine their compressive strength following the standard procedure ASTM C 39/C39M-09a (*Standard Test Method for Compressive Strength of Cylindrical Concrete Specimens*). Total porosity and absorption were calculated according to the standard procedure ASTM C642-06 (*Standard Test Method for Density, Absorption, and Voids in Hardened Concrete*), where the samples are dried then boiled in water to determine the total volume of permeable voids, after 28 and 90 days of curing. Capillary sorptivity was also assessed by applying the standard procedure EMPA – SIA 162/1 [36], in which water is allowed to pass into a dried sample through a more gradual process of capillary suction, and the mass of the sample is monitored as a function of time. The resistance to chloride ion penetration was determined in accordance with the standard procedure ASTM C1202-05 (*Standard Test Method for Electrical Indication of Concrete's Ability to Resist Chloride Ion Penetration*) using a *PROOVE'it* instrument supplied by *Germann Instruments*.

To study the carbonation of concrete specimens, an accelerated carbonation testing system was used. The conditions applied were: CO_2 concentration of 1.0 ± 0.2%, temperature of 25 ± 2 °C, and RH = 65 ± 5%. Comparable conditions were used in a previous study [31] by the authors to assess the carbonation mechanisms of paste and mortar specimens of the alkali-activated slag binder used in this study. Specimens were

Table 2
Mix designs studied. All quantities are in kg/m^3 of fresh concrete.

Component	AASC mixes – slag content			OPCC mixes – cement content		
	300 kg/m^3	400 kg/m^3	500 kg/m^3	300 kg/m^3	400 kg/m^3	500 kg/m^3
OPC	–	–	–	300	400	500
GBFS	300	400	500	–	–	–
Na silicate	111	148	185	–	–	–
Water	66	88	110	126	168	210
Sand	990	885	780	1010	913	815
Gravel	990	885	780	1010	913	815
Fresh paste volume fraction	0.241	0.321	0.402	0.225	0.300	0.375

covered with a polymer layer on the end faces of the cylindrical specimens, to drive the CO_2 ingress into the sample through the sides of the cylinder only. Before the test, samples were stored in the carbonation chamber for 48 h without CO_2, to stabilize the moisture according to the testing conditions. During CO_2 exposure, concrete specimens were removed from the chamber after 250, 500, 750 and 1000 h. The depth of carbonation was measured by treating the surface of a freshly cleaved specimen with a 1% solution of phenolphthalein in alcohol. In the uncarbonated part of the specimen, where the concrete was still highly alkaline, purple-red coloration was obtained, while no coloration is observed in the carbonated region. Each carbonation depth result presented is calculated as the distance from the sample edge to the point of color change, the average of between 7 and 14 measurements (7 points per sample on either one or two replicate samples).

3. Results and discussion

3.1. Compressive strength

Higher compressive strength is consistently observed in the concretes with larger amounts of binder (Fig. 1). Alkali silicate-activated concretes (AASC) and Portland cement concretes (OPCC) with 400 and 500 kg/m^3 of binder (i.e. slag for AASC, cement for OPCC) all show significantly higher strengths than the corresponding 300 kg/m^3 mixes at 28 days of curing, but 500 kg/m^3 does not in either case provide a significantly higher strength than the 400 kg/m^3 mix. This trend is maintained in the OPCC samples at 90 days of age. However, after 90 days of curing, AASC samples produced with 300 kg/m^3 of slag present compressive strengths comparable to the mixes with 400 kg/m^3, and slightly higher strength is obtained by using 500 kg/m^3 of slag.

The results obtained here for OPCC are in partial agreement with the data of Wassermann et al. [34], who found that the strengths of OPCC mixes at constant water to cement ratio (w/c) were independent of binder content within the range studied. However, those authors utilized superplasticizing admixtures, and worked at a minimum cement content of 372 kg/m^3 for their w/c 0.45 sample set. The 400–500 kg/m^3 samples assessed here are therefore within the range studied by those authors (although any direct numerical comparisons between the data sets need also to consider the effect of w/c on paste density), and the minimal observed differences in strength between these samples agree with their data. The 300 kg/m^3 OPCC samples in Fig. 1 appear to be too low in binder to reach the regime where strength is independent of binder content. However, it is of interest that: (a) the AASC samples do not show such a sharp transition from the regime where strength is dependent on binder content to the regime (at higher binder content) where strength and binder content are effectively independent, and (b) the effect of longer-term curing on this property is far more notable in AASC, indicating a more extended period of ongoing chemical reaction leading to strength generation during curing.

It is also notable that, regardless of the binder content, the AASC concretes assessed here report compressive strengths higher than 60 MPa after 90 days of curing, enabling the classification of these materials as high performance concretes (HPC). The achievement of such values of compressive strength in Portland cement-based concretes usually requires the addition of chemical and/or mineral admixtures [37].

The high mechanical strength of alkali-activated slag based-materials is attributed to the physical and structural characteristics of the binders formed in these systems. The hydration reactions of alkali-activated slag are controlled by dissolution and precipitation phenomena, whose kinetics at elevated pH are faster than the diffusion-controlled reaction processes which take place in Portland cement hydration [38,39], giving high compressive strengths at early ages of curing. The use of sodium silicate based-activators leads to the formation of binders whose structure is mainly a calcium silicate hydrate gel (C–S–H) [39–41], and this is the reaction product primarily responsible for strength development. During the alkali-activation reaction, the silicate ions which are both dissolved from the slag and supplied by the activator provide to the system the species necessary to promote reactions with the Ca released from the slag. As the reaction progresses further, the silicate ions supplied by the activator become depleted but slag dissolution continues. Condensation and cross-linking of these species leads to gelation, resulting in a calcium silicate hydrate type product with a low to moderate Ca/Si ratio, with some of the Si substituted by Al supplied by the slag, and also incorporating some alkalis into charge-balancing sites and sorbed onto the gel structure [39,40,42].

Secondary reaction products which can be observed in the alkali-activated slag binder include aluminosilicate phases related to zeolites, and hydrotalcite-type phases [39,41,43]. While the slag used here contains insufficient Mg to lead to the formation of hydrotalcite [31,44], the presence of a discrete calcium aluminosilicate gel has been observed within hardened paste samples of the same composition as the binders used here, via the identification of zeolite crystallites of the gismondine family by synchrotron X-ray diffractometry [31,44]. After longer periods of curing, the C–S–H gel of AASC exhibits an increased degree of polymerization and a higher degree of formation of reaction products [27]. This is in agreement with the presence of crystalline and highly-crosslinked phases such as gismondine in the samples, and is believed to contribute positively to the development of higher mechanical strengths at advanced ages of curing [27,44].

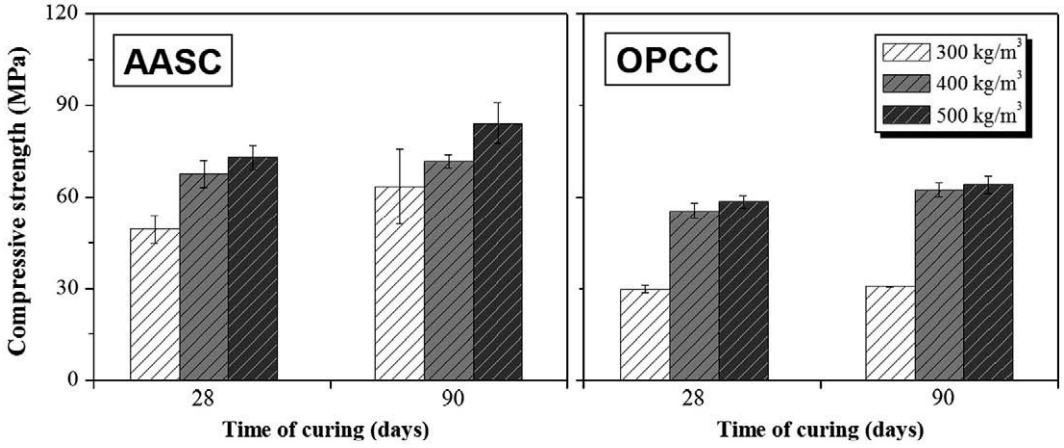

Fig. 1. Compressive strengths of alkali silicate-activated concretes as a function of the binder content. Error bars represent one standard deviation.

Table 3
Absorption and total porosity in AASC and OPCC concretes formulated with different contents of binder.

Type of concrete	Binder (slag or cement) content (kg/m^3)	Period of curing (days)			
		Water absorption (wt.%)		Volume of permeable voids (%)	
AASC		28	90	28	90
	300	5.4	4.2	13.0	9.8
	400	3.2	2.1	8.4	5.3
	500	4.7	3.0	11.1	7.4
OPCC	300	5.5	4.5	13.3	10.9
	400	5.1	4.3	11.9	10.4
	500	6.2	4.5	14.4	10.8

In AASC and other alkali-activated binders, the binder-aggregate interface (interfacial transition zone) has been reported to be highly dense and uniform, with only minimal differences between this region and the area of the binder further away from the aggregate particles [45]. This phenomenon also contributes to the high mechanical strength of alkali-activated concretes. The characteristics of the transition zone in alkali silicate-activated AASC can be attributed to several factors such as the refinement of the porosity by the condensation of the excess SiO_2 supplied by the activator, and also potentially the partial reaction of the surfaces of siliceous aggregates with the alkali silicate solution to form additional reaction products surrounding the aggregate particles. This promotes stronger bonding between the macro-phases through the reaction products formed around the aggregates, and the increased roughness of the particles also enhances mechanical linking [46,47]. It is important to note that this differs from the microstructure reported in OPCC, where the area between matrix and the aggregates is the weakest part of the material and is characterized by a high porosity [48].

3.2. Water absorption properties

3.2.1. Total porosity and absorption

AASC and OPCC samples with similar contents of binder show comparable water absorption values at both 28 and 90 days (Table 3). A reduction in the total porosity after 90 days of curing is identified in all samples, with AASC showing a more marked reduction than the reference OPCC. The total porosities of the 400 kg/m^3 binder content samples are much lower than the mixes with either higher or lower binder contents, for both the AASC and OPCC sample series. This is most likely due in part to particle packing issues within the concretes. The 300 kg/m^3 samples contain insufficient binder to enable full compaction, while on the other hand, the 500 kg/m^3 samples are more likely to suffer from microcracking due to excessive heat generation, which will be explored in more detail later in this paper. The aggregate gradings were not individually optimized for each binder content, which may also contribute to this behavior.

The binder content of the concretes has a particularly strong effect on the water absorption properties of AASC samples, although the water absorption values are, in all cases, lower than the comparable OPCC samples even where porosities are similar. This is probably a result of the presence of very refined, tortuous and closed porosity in the AASC samples [49], which water does not readily penetrate, and also the ongoing formation of reaction products at advanced ages of curing [44]. It may also be that some of the water that is absorbed into the OPCC samples participates in further hydration processes in these samples, which have reasonably low w/c ratios and therefore probably incomplete cement hydration.

The results in Table 3, showing variation in porosity as a function of time for each sample, are generally in good agreement with the mechanical strength development observed in the concretes, with the AASC mixes showing both more strength development and a more significant reduction in porosity from 28 to 90 days.

The permeability of concrete plays an important role in the ingress of various aggressive ions from the environment, and their movement through the material. It has been reported [50] that absorption values <3% and total porosity values <10% are able to be related to concretes with good durability. Based on this, it is possible to classify AASC samples produced with 400 and 500 kg/m^3 and cured for 90 days as concretes which have the potential to be highly durable, in comparison to the OPCC samples which report twice the values suggested by the standard for such a classification. However, more detailed analysis of water, chloride and carbonate ingress into these materials is necessary before such a conclusion may be definitively proclaimed.

3.2.2. Capillary sorptivity

Capillary sorptivity curves obtained for concretes with 28 days of curing and formulated with different amounts of binder are shown in Fig. 2. It can be seen that a higher content of binder in the AASC samples leads to significantly lower water absorption, which is coherent with a reduced porosity and a refined pore structure. These differences are more marked in AASC samples with 500 kg/m^3 of slag when compared with the behavior reported by the reference concrete (OPCC), whose increased absorption of water under these formulation conditions can, as for the data presented in Table 3, tentatively be attributed to microcracking induced in the sample by the higher heat release at high cement content. Although cracking of this sample was not visibly apparent during or after testing, the presence of some microcracks cannot be discounted, and is consistent with the observed behavior.

Understanding the apparent discrepancy in the behavior of the AASC sample with 500 kg/m^3 of binder requires the extraction of characteristic sorptivity parameters from the data in Fig. 2. The kinetics of the capillary sorption of water into concrete can be described by the capillary absorption coefficient (k) and the resistance

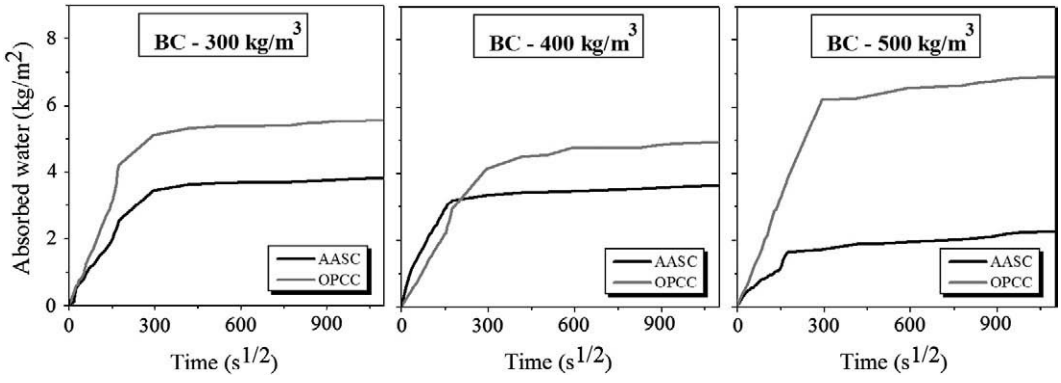

Fig. 2. Capillary sorptivity of 28-day cured AASC and OPCC concretes as a function of the binder content (BC).

Table 4
Capillary sorptivity coefficients of AASC and OPCC concretes as a function of binder content.

Type of concrete	Binder content (kg/m^3)					
	300	400	500	300	400	500
	m (s/m^2)$\times 10^7$			k (kg/m^{2}s$^{1/2}$)		
AASC	5.57	5.94	4.83	0.010	0.009	0.005
OPCC	5.27	5.41	4.61	0.015	0.012	0.018

to water penetration (m), both determined from the capillary sorptivity curves as recommended by Fagerlund [36]. Table 4 shows that the k values (the initial slopes of the sorptivity plots in Fig. 3) of AASC are very significantly lower than those of OPCC samples with similar binder contents, but there is little difference in m between corresponding AASC and OPCC samples.

It is also notable that for the AASC samples, k decreases by as much as 50% when moving from 300 to 500 kg/m^3 of slag, but that the resistance to water penetration $\left(m = \frac{\text{saturation time}}{(\text{penetration depth})^2}\right.$ with time in seconds and depth in meters) shows a much smaller variability. The resistance to water penetration increases, as expected, between samples produced with 300 and 400 kg/m^3; however, for both AASC and OPCC systems, an increased content of binder (500 kg/m^3) leads to a reduction in this property, indicating a decreased resistance to the total ingress of aggressive agents into the material.

These data may then be used to explain some of the microstructural differences between the AASC and OPCC samples. The total porosity of each sample controls its resistance to water penetration, is reasonably similar between the two sample sets, and shows a minimum (corresponding to a maximum in m) at 400 kg/m^3 in each case. The capillary absorption coefficient k, on the other hand, is more closely linked to total porosity and pore structure, being derived from the kinetics of water sorption in the time leading up to saturation of the pore network. The pore structure of the 300 kg/m^3 concrete contains more high-radius pores, as the binder content is insufficient to fully fill the spaces between the aggregate particles with dense reaction products. This is consistent with the lower strength of these concretes. Providing more binder (400 kg/m^3) enables filling of this space. The sorptivity values are also in good agreement with those reported by Wassermann et al. [34] for Portland cement concretes formulated with 200 kg/m^3 of water and cement contents between 313 and 450 kg/m^3.

The highest binder content, 500 kg/m^3, could cause thermally induced microcracking in the OPCC samples, which would give a reduced m and an increased k due to the presence of more and larger voids than in the 400 kg/m^3 sample. The same binder content in AASC does lead to increased total porosity and water absorption (Table 3) and slightly reduced resistance to water penetration (Table 4), but this effect appears to be insufficient to cause an increase in the capillary sorptivity, k; this parameter actually decreases significantly between 400 and 500 kg/m^3. The reason for this may lie in the differences between the ASTM C642-06 and EMPA-SIA 162/1 test methodologies, where the ASTM test (Table 3) involves boiling the sample to rapidly determine water absorption, whereas the EMPA method (Table 4) is a less aggressive test where the water is allowed to be absorbed into a dried sample by natural capillary action.

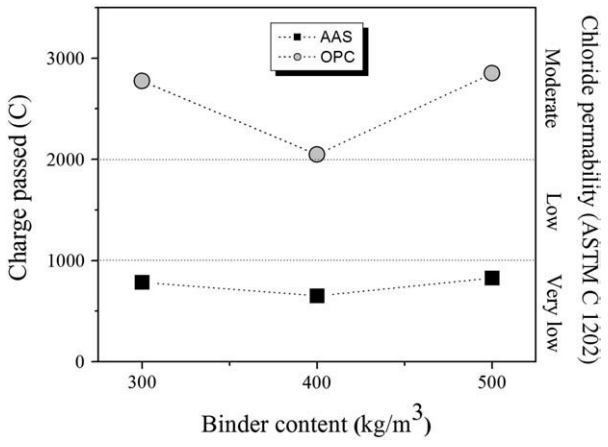

Fig. 3. Rapid chloride permeability test results for 28-day cured AASC and OPCC concretes as a function of the binder content.

3.3. Rapid chloride permeability testing

Chloride permeability of the concrete samples was assessed according to the rapid chloride permeability test, ASTM C1202, and the values of total transferred charge for 28-day cured samples are shown in Fig. 3. It can be seen that the AASC samples exhibit a much lower charge passed, which (under the assumptions of the test method) corresponds to a reduced permeability of chloride ions, compared with the reference OPCC samples. Based on these results and according to the ASTM C1202 classification of concretes, all AASC samples tested are classified as concretes with very low permeability to chlorides, while these OPCC samples belong to the category of concretes with moderate permeability to chlorides.

Slight differences in the amounts of charge passed by AASC produced with different amounts of binder are identified; however, OPCC samples show more variability between samples. An increase in charge passed correlates with a reduced resistance to water penetration (at 300 and 500 kg/m^3 of binder content), further showing that formulating OPCC with 400 kg/m^3 of binder seems to be an optimum value that leads to an improvement in the sorptivity properties of these materials with the aggregate blend and w/c ratio assessed here.

However, in the interpretation of data obtained by the rapid chloride permeability test, it is important to take into account that this test is fundamentally a measurement of the electrical conductivity of concretes. Ionic transport is strongly dependent on the pore network structure in the binder matrix, while electrical conductivity in concrete is affected by both the pore network structure and the chemical composition of the pore solutions [51]. In alkali-activated slag binders, it has been identified that the pore solutions contain high concentrations of ionic species, mainly Na^+ and OH^- [52–55], which will influence the results of the test.

Any Na^+ present in the pores of the material will be expected to counter-diffuse as the Cl^- ions are electrically driven into the pore network, leading to an increased charge transfer during the test. This suggest that the values obtained from this test are able to be considered as an indicator for quality control of concretes when comparing materials produced with similar binder chemistry and therefore comparable pore solution compositions, rather than comparing across binder types [51,56].

Thus, it may be expected that a higher ionic strength in the pore solution of the samples would lead to increased charge passed values, meaning that the values observed in the AASC specimens assessed could be higher than the actual chloride permeability that is taking place in reality. It has also been observed that blending cement with high levels of supplementary cementitious materials (including slag) causes a reduction in charge passed which exceeds the improvement in chloride mobility as measured by ponding tests [51], and previous tests of alkali-activated slags using the ASTM C1202 test have shown unexpectedly low charge passed when compared to other means of assessing transport properties of mortars [57]. Differences in the formation of interfacial transition zones between the mortars used in that investigation and the concrete samples studied here may lead to some differences in the details of electrical conductivity and chloride

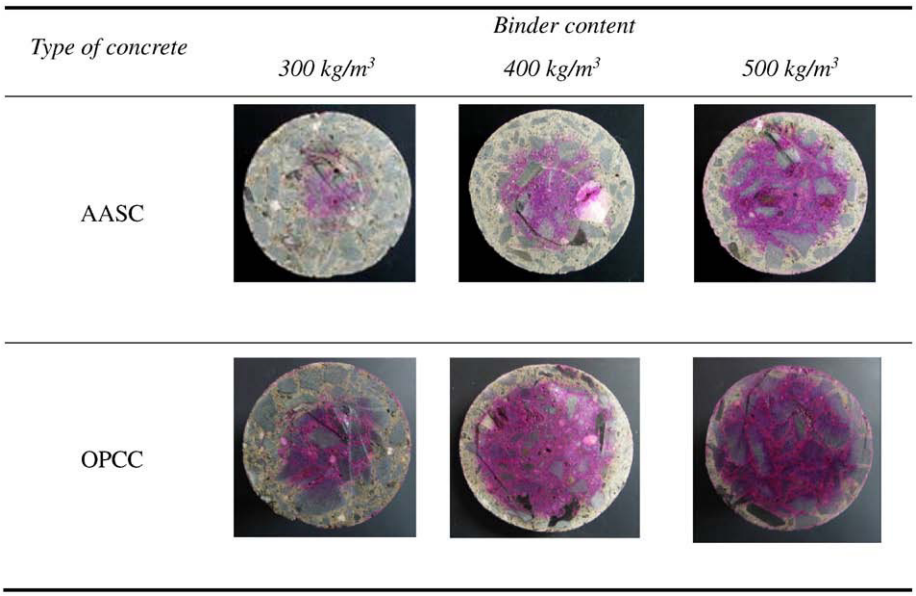

Fig. 4. Transverse sections of carbonated concretes after 1000 h of exposure to a 1% CO_2 environment, with the extent of carbonation revealed by a phenolphthalein indicator. Samples are 76.2 mm in diameter.

permeability, but the general trends observed should be expected to be consistent.

Therefore, further analysis (including modeling) of the exact applicability of the rapid chloride permeability test to alkali-activated binder systems is certainly desirable to resolve these issues, but the results obtained here do appear to agree with the capillarity and water absorption measurements presented above, in showing that the AASC mixes are potentially highly durable.

3.4. Carbonation

The carbonation of Portland cement (OPC) mortar and concrete is a widely studied and reasonably well-understood phenomenon. Carbon dioxide from the atmosphere diffuses inside the material and dissolves in the pore water, forming carbonic acid. Carbonic acid may then attack calcium-containing phases. Initially the calcium hydroxide ($Ca(OH)_2$), and then calcium silicate hydrates (C–S–H) and calcium aluminosilicate hydrates (C–A–S–H), are decalcified by reactions which extract their calcium to form calcium carbonate. $Ca(OH)_2$ in particular plays a buffering role by releasing hydroxide into the pore solution as the pH begins to decrease, but it will at some point become depleted and no longer able to maintain this buffering. This may lead, in the long-term, to a reduction in the alkalinity of the cementitious system accompanied by reduced mechanical performance and the corrosion of steel reinforcement [18–22,58]. Throughout CO_2 exposure of AAS binders, the main reaction products are expected to be carbonates (in particular calcite and trona [31]) derived from the carbonation of alkaline pore solutions and C–A–S–H gels.

An illustration of the extent of carbonation observed in the concrete samples studied is shown in Fig. 4. In AASC samples, a significant effect of binder content on the rate of carbonation is visible in Fig. 4, and is displayed in Fig. 5A as a function of the time of exposure to CO_2. Similar to the trend observed in OPCC samples (Fig. 5B), lower carbonation depths are observed in concretes with higher binder contents.

A reduced binder content of 300 kg/m^3 led to a very significant increase in the carbonation rate of both AASC and OPCC when compared with the samples with higher binder contents. After 250 h of exposure, the 300 kg/m^3 AASC mix exhibited a carbonation depth six times greater than those observed in the other AASC mixes at the same time. Conversely, a higher binder content (400 or 500 kg/m^3) leads to a lower progress of carbonation in AASC samples, which correlates well with the reduced water permeability identified in these samples, while in OPCC no differences are observed in the carbonation rates of concretes formulated with 400 or 500 kg/m^3 of binder. The known susceptibility

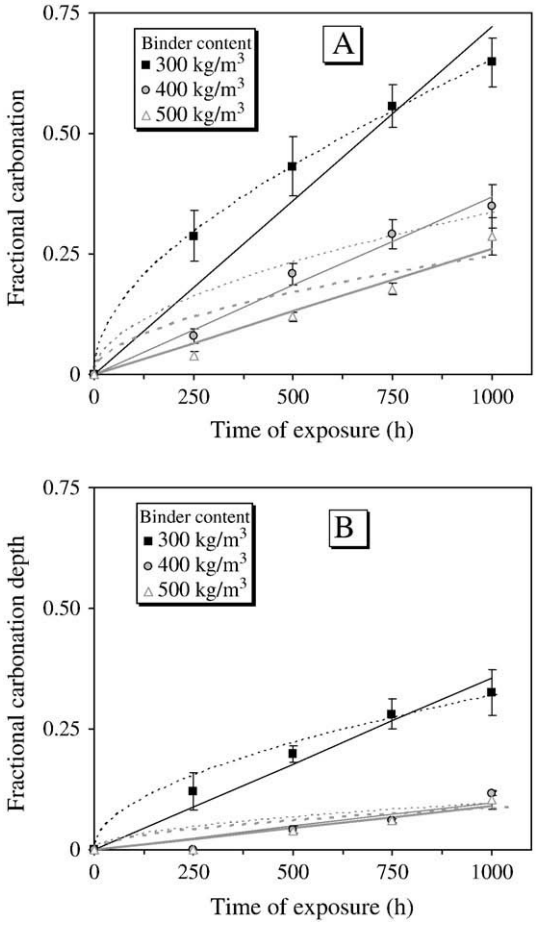

Fig. 5. Carbonation depth as function of the amount of binder of concretes based on (A) alkali-activated GBFS and (B) Portland cement. Dashed lines represent the best fit of the diffusion control model to each data set, and solid lines are the best fit of the chemical reaction control model. Error bars represent one standard deviation.

of AAS binders to carbonation, which is generally ascribed to their higher alkali content, agrees with the fact that these samples show a higher extent of carbonation than the OPCC samples at lower times of exposure. The 400 and 500 kg/m^3 OPCC samples did not show an observable carbonated region on the sample surfaces after 250 h; it is unlikely that the extent of carbonation was in fact zero, but the carbonated depth was too low to be visually observed. In both sample sets, the rate of carbonation correlate well with what would be expected from the trends in compressive strength, but less closely with the observed microstructural and pore structure parameters. This indicates that the fundamental binder chemistry and distribution are more critical to carbonation resistance than are the details of the pore network, under the conditions of this study.

This observation leads to the suggestion that the common assumption that carbonation is diffusion-controlled [23,59] may not apply in this case. Fig. 5 therefore shows the results of fitting both diffusion-controlled and chemical reaction-controlled "shrinking core" type models [60] to the carbonation data. The models were applied to the data using the assumption of cylindrical geometry with no end effects (pseudo-infinite cylinders), which is appropriate given that the sample ends were sealed to prevent carbonate ingress from these surfaces. For this geometry, the form of the chemical reaction control model (with the assumption of a first-order chemical reaction) is given by Eq. (1), and the diffusion control model by equation (2), where X is the fractional volume carbonated and τ is the time required for complete carbonation [60]:

$$\frac{t}{\tau} = 1-(1-X)^{1/2} \quad (1)$$

$$\frac{t}{\tau} = X + (1-X)\ln(1-X) \quad (2)$$

Using the relationship between X and the fractional carbonated radius r_c, $X = 1-(1-r_c)^2$, in Eqs. (1) and (2), and fitting the parameter τ in each equation by minimizing the sum of squared errors, gives the model curves plotted in Fig. 5.

It can be seen from Fig. 5 that the diffusion control model fits the 300 kg/m^3 data for the AASC samples very well, but provides a poor description of the other data sets. Conversely, the chemical reaction control model fits the 400 and 500 kg/m^3 data for both sample sets very well, but is unable to provide an adequate description of the 300 kg/m^3 data. From these outcomes, and also by observing the deviations of the 300 kg/m^3 OPCC data set from the predictions of either model, some empirical observations regarding the mechanisms controlling carbonation can be made:

(1) For carbonation depths of up to approximately 8 mm (~20% carbonation depth in Fig. 5), the carbonation process of both the OPCC and AASC samples appears to be predominantly chemical reaction controlled, and the rate-controlling step is close to first order with respect to CO_2. The exact nature of the rate-controlling chemical reaction remains to be determined, although it seems likely that the absorption of CO_2 into the pore solution will be slower than any of the chemical reactions involving the dissolved CO_2 once it has entered the pore solution.

(2) Once the carbonation depth becomes greater than this, diffusion of dissolved CO_2 through the pore network of the carbonated layer becomes dominant in determining the rate of further carbonation. This is shown by the good fit of the diffusion control model to the 300 kg/m^3 AASC data set, which rapidly passes 20% carbonation and therefore does not display an extended period of chemical reaction control to introduce deviations from the diffusion control model. However, the 300 kg/m^3 OPCC mix does not carbonate as rapidly in the initial stages of the reaction, which means that it is likely to be under a combination of rate controlling mechanisms: chemical reaction control initially, with diffusional resistances becoming more dominant as carbonation proceeds. The data for this sample fall between the predictions of the two models in Fig. 5B. It is possible to envisage that an improved model fit to these data could be obtained by the use of a relatively rapid chemical reaction controlled process with a gradually increasing mass transfer resistance; however, such modeling is beyond the scope of the current analysis.

(3) The presence of microcracking in the 500 kg/m^3 OPCC sample, as inferred from porosimetry and capillarity data, does not appear to accelerate the progression of the carbonation front through this sample. This suggests that the carbonation products may be filling some of the voids (including microcracks) within the sample as carbonation continues, meaning that this sample does not carbonate any more rapidly than the (presumably uncracked) 400 kg/m^3 sample. However, the 500 kg/m^3 AASC sample carbonates less rapidly than its 400 kg/m^3 counterpart, meaning that the microcracking of the OPCC sample seems to be causing some loss of potential performance. The intrinsic binder porosity in both 300 kg/m^3 samples is too high for the effect of pore blocking by carbonate products to be significant.

Although this is a simplistic analysis, and there are numerous more sophisticated models available in the literature which describe the various aspects of the carbonation process in mechanistic detail, the information obtained is certainly of value in understanding the differences and similarities in carbonation of AASC and OPCC.

4. Conclusions

By analysis of concretes prepared at a range of binder contents, using either alkali silicate-activated slag or Portland cement as binder materials, the effects of concrete mix design on mechanical and durability performance have been determined. For comparable binder contents and water/binder ratios, alkali-activated slag concretes generate higher strengths at both 28 and 90 days, and the strength data obtained are less sensitive to binder content. The alkali-activated slag concretes also display lower water absorption, total porosity and capillarity at comparable binder content, and these properties decrease with increasing binder content. Microcracking at high binder content is less evident in the alkali-activated concretes due to the lower heat release of this binder, and is apparent due to differences in capillarity and strength data. The apparent resistance to chloride penetration, as measured by the charge passed in an electrically accelerated test, appears very high (i.e. low charge passed) in all alkali-activated concrete samples, although the interpretation of the results of this test is not yet certain for concretes, such as these, which contain very high levels of supplementary cementitious materials. Although higher susceptibility to carbonation has been identified in alkali-activated slag concretes, improvements can be obtained by controlling mix design so that the resistance to carbonation approaches that of Portland cement concretes.

Acknowledgments

This study was sponsored by *Universidad del Valle* (Colombia), *Instituto Colombiano para el Desarrollo de la Ciencia y Tecnología "Francisco José de Caldas"* (COLCIENCIAS) and the Center of Excellence of Novel Materials (CENM). The participation of JLP was funded by the Australian Research Council (ARC), including partial funding through the Particulate Fluids Processing Centre, a Special Research Centre of the ARC.

References

[1] F. Puertas, Cementos de escoria activados alcalinamente: situación actual y perspectivas de futuro, Mater Constr 45 (239) (1995) 53–64.
[2] D. Roy, Alkali-activated cements – opportunities and challenges, Cem. Concr. Res. 29 (2) (1999) 249–254.
[3] C. Shi, P.V. Krivenko, D.M. Roy, Alkali-activated cements and concretes, Taylor & Francis, Abingdon, UK, 2006.

[4] B. Talling, P.V. Krivenko, Blast furnace slag – the ultimate binder, in: S. Chandra (Ed.), Waste Materials Used in Concrete Manufacturing, Noyes Publications, Park Ridge, NJ, 1997, pp. 235–289.
[5] S.-D. Wang, X.-C. Pu, K.L. Scrivener, P.L. Pratt, Alkali-activated slag cement and concrete: a review of properties and problems, Adv. Cem. Res. 7 (27) (1995) 93–102.
[6] J.L. Provis, J.S.J. van Deventer (Eds.), Geopolymers: Structures, Processing, Properties and Industrial Applications, Woodhead, Cambridge, UK, 2009, p. 448.
[7] J.S.J. van Deventer, J.L. Provis, P. Duxson, D.G. Brice, Chemical research and climate change as drivers in the commercial adoption of alkali activated materials, Waste Biomass Valoriz 1 (1) (2010) 145–155.
[8] T. Bakharev, J.G. Sanjayan, Y.-B. Cheng, Alkali activation of Australian slag cements. Cem. Concr. Res. 29 (1) (1999) 113–120.
[9] F. Collins, J.G. Sanjayan, Microcracking and strength development of alkali activated slag concrete, Cem. Concr. Compos. 23 (2001) 345–352.
[10] F. Collins, J.G. Sanjayan, Workability and mechanical properties of alkali-activated slag concrete, Cem. Concr. Res. 29 (1999) 455–458.
[11] D. Hardjito, S.E. Wallah, D.M.J. Sumajouw, B.V. Rangan, On the development of fly ash-based geopolymer concrete, ACI Mater. J. 101 (6) (2004) 467–472.
[12] D.M.J. Sumajouw, D. Hardjito, S.E. Wallah, B.V. Rangan, Fly ash-based geopolymer concrete: study of slender reinforced columns, J. Mater. Sci. 42 (9) (2007) 3124–3130.
[13] M. Sofi, J.S.J. van Deventer, P.A. Mendis, G.C. Lukey, Engineering properties of inorganic polymer concretes (IPCs), Cem. Concr. Res. 37 (2) (2007) 251–257.
[14] S.A. Bernal, M. Gordillo, R. Mejía de Gutiérrez, E. Rodríguez, S. Delvasto, R. Cuero, Modeling of the compressive strength of alternative concretes using the response surface metholodogy, Rev. Fac. Ing. Univ. Antioquia 49 (2009) 112–123.
[15] S.A. Bernal, R. Mejía de Gutiérrez, S. Delvasto, E. Rodríguez, Performance of an alkali-activated slag concrete reinforced with steel fibers, Constr. Build. Mater. 24 (2) (2010) 208–214.
[16] E. Rodríguez, S. Bernal, R. Mejía de Gutiérrez, S. Delvasto, Concretos alternativos basados en GBFS, Mater. Constr. 58 (291) (2008) 53–67.
[17] I.V. Belitsky, Design of slag-alkaline concrete mixes, in: P.V. Krivenko (Ed.), Proceedings of the First International Conference on Alkaline Cements and Concretes, VIPOL Stock Company, Kiev, Ukraine, 1994, pp. 864–869.
[18] F.P. Glasser, J. Marchand, E. Samson, Durability of concrete — degradation phenomena involving detrimental chemical reactions, Cem. Concr. Res. 38 (2) (2008) 226–246.
[19] D.W. Hobbs, Concrete deterioration: causes, diagnosis, and minimising risk, Int. Mater. Rev. 46 (3) (2001) 117–144.
[20] V.G. Papadakis, C.G. Vayenas, M.N. Fardis, Experimental investigation and mathematical modeling of the concrete carbonation problem, Chem. Eng. Sci. 46 (1991) 1333–1338.
[21] A. Poonguzhali, H. Shaikh, R.K. Dayal, H.S. Khatak, Degradation mechanism and life estimation of civil structures – a review, Corros. Rev. 26 (4) (2008) 215–294.
[22] A. Steffens, Modeling carbonation for corrosion risk prediction of concrete structures, Cem. Concr. Res. 32 (2002) 938–941.
[23] V.G. Papadakis, C.G. Vayenas, M.N. Fardis, A reaction engineering approach to the problem of concrete carbonation, AIChE J. 35 (10) (1989) 1639–1650.
[24] J. Deja, Carbonation aspects of alkali activated slag mortars and concretes, Silic. Ind. 67 (1) (2002) 37–42.
[25] V.P. Ilyin, Durability of materials based on slag-alkaline binders, in: P.V. Krivenko (Ed.), Proceedings of the First International Conference on Alkaline Cements and Concretes, VIPOL Stock Company, Kiev, Ukraine, 1994, pp. 789–836.
[26] F. Puertas, M. Palacios, T. Vázquez, Carbonation process of alkali-activated slag mortars, J. Mater. Sci. 41 (2006) 3071–3082.
[27] H. Xu, J.L. Provis, J.S.J. van Deventer, P.V. Krivenko, Characterization of aged slag concretes, ACI Mater. J. 105 (2) (2008) 131–139.
[28] S.A. Bernal, E. Rodríguez, R. Mejía de Gutiérrez, V. Rose, F. Puertas, S. Delvasto, Carbonation behavior of mortar produced by alkali-activation of a granulated-blast furnace slag, Proceedings of 23rd International Conference on Solid Waste Technology and Management, Widener University, Philadelphia, PA, 2008, CD-ROM proceedings.
[29] M. Criado, A. Palomo, A. Fernández-Jiménez, Alkali activation of fly ashes. Part 1: Effect of curing conditions on the carbonation of the reaction products, Fuel 84 (16) (2005) 2048–2054.
[30] M. Palacios, F. Puertas, Effect of carbonation on alkali-activated slag paste, J. Am. Ceram. Soc. 89 (10) (2006) 3211–3221.
[31] S.A. Bernal, R. Mejía de Gutierrez, V. Rose, J.L. Provis, Effect of silicate modulus and metakaolin incorporation on the carbonation of alkali silicate-activated slags, Cem. Concr. Res. 40 (6) (2010) 898–907.
[32] S. Bernal, E. Rodríguez, R. Mejía de Gutiérrez, J. Maldonado, Properties of alkali-activated slag concrete, in: Proceedings of the Brazilian Conference on Nonconventional Materials and Technologies: Affordable Housing and Infra-structures (NOCMAT), 2004, Pirassununga, Brazil, CD-ROM proceedings.
[33] L. Basheer, J. Kropp, D.J. Cleland, Assessment of the durability of concrete from its permeation properties: a review, Constr. Build. Mater. 15 (2001) 93–103.
[34] R. Wassermann, A. Katz, A. Bentur, Minimum cement content requirements: a must or a myth? Mater. Struct. 42 (7) (2009) 973–982.
[35] B. Bary, A. Sellier, Coupled moisture—carbon dioxide–calcium transfer model for carbonation of concrete, Cem. Concr. Res. 34 (2001) 1859–1872.
[36] G. Fagerlund, On the capillarity of concrete, Nord. Concr. Res. 1 (1982) 6.1–6.20.
[37] P.C. Hewlett, Lea's chemistry of cement and concrete, 4th Ed.Elsevier, Oxford, UK, 1998.
[38] D.M. Roy, M.R. Silsbee, Alkali activated materials. An overview, Mater. Res. Soc. Symp. Proc. 245 (1992) 153–164.
[39] S.D. Wang, K.L. Scrivener, Hydration products of alkali-activated slag cement, Cem. Concr. Res. 25 (3) (1995) 561–571.
[40] A. Fernández-Jiménez, F. Puertas, Structure of calcium silicate hydrates formed in alkaline-activated slag: influence of the type of alkaline activator, J. Am. Ceram. Soc. 86 (8) (2003) 1389–1394.
[41] I.G. Richardson, A.R. Brough, G.W. Groves, C.M. Dobson, The characterization of hardened alkali-activated blast-furnace slag pastes and the nature of the calcium silicate hydrate (C–S–H) paste, Cem. Concr. Res. 24 (5) (1994) 813–829.
[42] S.-D. Wang, K.L. Scrivener, ^{29}Si and ^{27}Al NMR study of alkali-activated slag, Cem. Concr. Res. 33 (5) (2003) 769–774.
[43] P.V. Krivenko, Alkaline cements, in: P.V. Krivenko (Ed.), Proceedings of the First International Conference on Alkaline Cements and Concretes, VIPOL Stock Company, Kiev, Ukraine, 1994, pp. 11–129.
[44] S.A. Bernal, J.L. Provis, R. Mejía de Gutierrez, V. Rose, Evolution of binder structure in sodium silicate-activated slag-metakaolin blends, Cem. Concr. Compos, Cem. Concr. Res. 33 (1) (2011) 46–54.
[45] J.L. Provis, Y. Muntingh, R.R. Lloyd, H. Xu, L.M. Keyte, L. Lorenzen, P.V. Krivenko, J.S.J. van Deventer, Will geopolymers stand the test of time? Ceram. Eng. Sci. Proc. 28 (9) (2007) 235–248.
[46] W.K.W. Lee, J.S.J. van Deventer, Chemical interactions between siliceous aggregates and low-Ca alkali-activated cements, Cem. Concr. Res. 37 (6) (2007) 844–855.
[47] C. Shi, Interface between cement paste and quartz sand in alkali-activated slag mortars, Cem. Concr. Res. 28 (6) (1998) 887–896.
[48] J.P. Ollivier, J.C. Maso, B. Bourdette, Interfacial transition zone in concrete, Adv. Cem. Based Mater. 2 (1) (1995) 30–38.
[49] F. Collins, J.G. Sanjayan, Effect of pore size distribution on drying shrinking of alkali-activated slag concrete, Cem. Concr. Res. 30 (9) (2000) 1401–1406.
[50] O. Trocónis de Rincón, Manual for inspecting, evaluating and diagnosing corrosion in reinforced concrete structures, DURAR Thematic Network XV.B. Durability of rebars, CYTED Iberoamerican Program Science and Technology for Development, Maracaibo, Venezuela, 2000.
[51] C. Shi, Another look at the rapid chloride permeability test (ASTM C1202 or ASSHTO T277), FHWA Resource Center, Baltimore, 2003.
[52] A. Gruskovnjak, B. Lothenbach, L. Holzer, R. Figi, F. Winnefeld, Hydration of alkali-activated slag: comparison with ordinary Portland cement, Adv. Cem. Res. 18 (3) (2006) 119–128.
[53] R.R. Lloyd, J.L. Provis, J.S.J. van Deventer, Pore solution composition and alkali diffusion in inorganic polymer cement, Cem. Concr. Res. 40 (9) (2010) 1386–1392.
[54] F. Puertas, A. Fernández-Jiménez, M.T. Blanco-Varela, Pore solution in alkali-activated slag cement pastes. Relation to the composition and structure of calcium silicate hydrate, Cem. Concr. Res. 34 (2004) 139–148.
[55] S. Song, H.M. Jennings, Pore solution chemistry of alkali-activated ground granulated blast-furnace slag, Cem. Concr. Res. 29 (1999) 159–170.
[56] C. Shi, Effect of mixing proportions of concrete on its electrical conductivity and the rapid chloride permeability test (ASTM C1202 or ASSHTO T277) results, Cem. Concr. Res. 34 (3) (2004) 537–545.
[57] C. Shi, Strength, pore structure and permeability of alkali-activated slag mortars, Cem. Concr. Res. 26 (12) (1996) 1789–1799.
[58] B. Johannesson, P. Utgenannt, Microstructural changes caused by carbonation of cement mortar, Cem. Concr. Res. 31 (2001) 925–931.
[59] M. Castellote, C. Andrade, Modelling the carbonation of cementitious matrixes by means of the unreacted-core model, UR-CORE, Cem. Concr. Res. 38 (12) (2008) 1374–1384.
[60] O. Levenspiel, Chemical Reaction Engineering, 3rd ed.Wiley, New York, 1999.